6-14-2022

Grotthuss Molecular Dynamics Simulations for Modeling Proton Hopping in Electrosprayed Water Droplets.

Lars Konermann

Scott Kim

Grotthuss Molecular Dynamics Simulations for Modeling Proton Hopping in Electrosprayed Water Droplets

Lars Konermann* and Scott Kim

Department of Chemistry, The University of Western Ontario, London, Ontario, N6A 5B7, Canada.

* corresponding author

E-mail address of the corresponding author: konerman@uwo.ca

Funding was provided by the Natural Sciences and Engineering Research Council of Canada (RGPIN-2018-04243).

ABSTRACT: Excess protons in water exhibit unique transport properties because they can rapidly hop along H-bonded water wires. Considerable progress has been made in unraveling this Grotthuss diffusion mechanism using QM-based computational techniques. Unfortunately, high computational cost tends to restrict those techniques to small systems and short times. Molecular dynamics (MD) simulations can be applied to much larger systems and longer time windows. However, standard MD methods do not permit the dissociation/formation of covalent bonds, such that Grotthuss diffusion cannot be captured. Here we bridge this gap by combining atomistic MD simulations (using Gromacs and TIP4P/2005 water) with proton hopping. Excess protons are modeled as hydronium ions that undergo $H_3O^+ + H_2O \rightarrow H_2O + H_3O^+$ transitions. In accordance with *ab initio* MD data, these Grotthuss hopping events are executed in "bursts" with quasi-instantaneous hopping across one or more waters. The bursts are separated by regular MD periods during which H_3O^+ ions undergo Brownian diffusion. The resulting proton diffusion coefficient agrees with the literature value. We apply this Grotthuss MD technique to highly charged water droplets that are in a size regime encountered during electrospray ionization (5 nm radius, ~17000 H_2O). The droplets undergo rapid solvent evaporation and occasional H_3O^+ ejection, keeping them at *ca*. 81% of the Rayleigh limit. The simulated behavior is consistent with phase Doppler anemometry data. The Grotthuss MD technique developed here should be useful for modeling the behavior of various proton-containing systems that are too large for high-level computational approaches. In particular, we envision future applications related to electrospray processes, where earlier simulations used metal cations while in reality excess protons dominate.

Introduction

The behavior of protons in aqueous solution (H^+_{aq}) has fascinated researchers for generations. Protonation/deprotonation modulates the behavior of proteins and other biomolecules. Proton transfer is also an integral part of energy conversion in biology[1] and technology.[2] The exact properties of H^+_{aq} remain under investigation, although recent work has resulted in many advances.[3-8] One proposed form of H^+_{aq} is the Eigen cation ($H_3O^+ \cdot 3H_2O$), where the central hydronium is H-bonded to three waters.[9] Alternatively, in the Zundel cation, a proton is bound between two waters.[10] Recent IR experiments[11, 12] and computational investigations[6, 8, 13, 14] revealed the prevalence of Eigen cations. In solution, these H_3O^+ ions have a slightly distorted structure where one H_2O is closer than the other two. The identity of this closest ligand fluctuates among the three water molecules on a sub-ps time scale, a process referred to as "special pair dance".[8, 13-17]

The transport properties of H_3O^+ are unique, with a diffusion coefficient that is roughly one order of magnitude larger than that of other small cations such as Li^+ or Na^+.[18] The latter undergo vehicular diffusion (Brownian motion).[19, 20] In contrast, H_3O^+ is subject to both Brownian motion and Grotthuss diffusion. The Grotthuss mechanism allows protons to rapidly migrate through water as a charge defect, by swapping covalent bonds for H-bonds.[21-27] Scheme 1 indicates how this mechanism can result in H_3O^+ translation along a H-bonded water wire.[28-30] Liquid water contains an extensive branched network of such water wires because each H_2O is ligated by ~four other H_2O molecules, albeit in a highly dynamic fashion.[31-34]

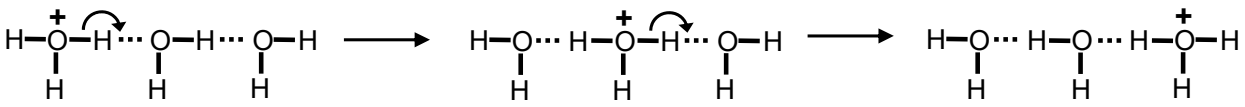

Scheme 1: Cartoon description of Grotthuss diffusion.[22] Straight solid lines indicate covalent bonds; dotted lines represent H-bonds. This simplistic scheme omits many details such as dynamic changes in H_3O^+ solvation during proton transfer. Also, bond angles are not properly reflected.

Modeling these Grotthuss events from first principles is not straightforward. Techniques that have been applied in this context include *ab initio* molecular dynamics (AIMD) where potentials are calculated on the fly using density functional theory,[6, 8, 14, 35-37] QM/MM methods,[28, 38, 39] multistate empirical valence bond (MS-EVB) simulations,[8] λ-dynamics,[40] and other approaches.[38, 41] While these techniques have uncovered many atomistic details, high computational cost tends to restrict their application to short times (picoseconds) and small systems, often less than 100 waters with a single H_3O^+.[8, 14, 28, 35, 36, 38, 42] Some studies were able to extend this range to significantly more water molecules and longer times[43] particularly when using MS-EVB and related approaches (see[2, 44-46] and references therein). Efforts to use simplified reactive force fields have yielded interesting data as well.[19, 20, 47-50] Nonetheless, simulations of large systems that involve Grotthuss diffusion remain challenging.

An area that would particularly benefit from a better understanding of H_3O^+ dynamics are highly charged water nanodroplets that play a central role in electrospray ionization (ESI) mass spectrometry.[51-54] This technique is used in countless laboratories for a wide range of applications.[55, 56] ESI initially converts analyte solution into a plume of charged droplets. After several cycles of solvent evaporation and fission, progeny droplets with radii of a few nm are generated.[57, 58] Throughout these events the droplets stay close to the Rayleigh limit where the number of charges is $z_R = 8\pi/e \times (\varepsilon_0 \gamma r^3)^{1/2}$ [r = radius, γ = surface tension, e = elementary charge].[57, 59-61] H_3O^+ ions generated by water oxidation ($6\ H_2O \rightarrow 4\ H_3O^+ + O_2 + 4e^-$) are the main source of droplet charge in positive ESI.[62] H_3O^+ from organic acids and other cations can contribute as well.[57] ESI nanodroplets liberate gaseous $[M + zH]^{z+}$ analyte ions which are then analyzed by a mass spectrometer.[55, 57, 63]

The central role of H_3O^+ as charge carrier in ESI nanodroplets implies that ESI mechanistic studies should account for Grotthuss diffusion, as noted in several recent studies.[51-54] Unfortunately, this aspect has been largely ignored in the ESI literature. ESI nanodroplets contain roughly 10^4 - 10^5

solvent molecules, and the time range of interest stretches over nano- to microseconds.[57] This size and temporal regime precludes the application of existing Grotthuss simulation methods.[8, 14, 19, 20, 28, 35, 36, 42-44, 47-49] There have been numerous recent efforts to study ESI nanodroplets using MD simulations.[63-72] Most of those simulations focused on droplets charged with metal ions such as Na^+ that can be modeled with standard MD force fields.[63-72] However, $[M + zNa]^{z+}$ ions generated in such simulations are of limited relevance for practical ESI conditions, where $[M + zH]^{z+}$ species dominate (implying that interactions with H_3O^+ are an essential component of analyte charging).[57] A handful of MD studies examined droplets containing H_3O^+, but this was done by treating these ions as Brownian particles without Grotthuss diffusion and without allowing for protonation/deprotonation events.[64, 67, 71, 73]

Clearly, the inclusion of Grotthuss diffusion in MD studies of ESI droplets and other large systems would be a significant advance. Here we address this challenge by combining classical MD simulations with proton hopping. Our method is not meant to capture all the atomistic details of individual hopping events. An accurate description of the ultrarapid (sub-ps) bond dissociation/formation and H_3O^+ solvation dynamics requires QM-based techniques.[6, 8, 14, 28, 35-39] Instead, by taking a somewhat simplified view of these events, we greatly extend the system size and time window accessible to Grotthuss simulations. The performance of our technique is illustrated by applying it to ESI nanodroplets containing ~17000 water molecules over tens of nanoseconds. The rapidly evaporating droplets represent non-equilibrium systems, where proton movement and ion ejection are strongly affected by electrostatic repulsion among numerous excess charges.[57, 59, 60] The Grotthuss MD approach presented here opens the door to future simulations on ESI events, as well as other processes involving H_3O^+ in aqueous solution.

Methods

General Strategy. Our MD simulations employed TIP4P/2005 water[74] (Figure S1A) which matches the water surface tension over a wide temperature range,[75] as required for realistic droplet simulations.[57, 63] A TIP4P/2005-compatible H_3O^+ model (Figure S1B) was generated based on refs.[76, 77] In itself, this model (like other H_3O^+ parametrizations)[64, 71, 73] is *not* capable of Grotthuss diffusion, because it does not allow for covalent bond dissociation/formation.[78, 79] The TIP4P/2005-based framework nonetheless represents a good starting point, because we found it to successfully capture several features. (1) Each H_3O^+ assembles an Eigen ($H_3O^+ \cdot 3H_2O$) solvation shell (Figure S2A),[9] consistent with experimental[11, 12] and computational data.[6, 8, 13, 14] (2) These Eigen complexes have a distorted structure with different lengths for the three H-bonds (see Figure S3: 0.171 nm, 0.183 nm, and 0.201 nm). This asymmetric solvation gives rise to a "special pair", representing the H_3O^+ and its closest H_2O ligand.[8, 13, 80] (3) The identity of this closest H_2O fluctuates among the three water ligands on a sub-ps time scale ("special pair dance", Figure S2B).[8, 13-17]

Grotthuss diffusion was incorporated by dissecting simulation runs into short segments. Each segment was conducted using standard MD with non-dissociable covalent bonds. At the end of each segment, all protons were allowed to hop (Scheme 1) while keeping the positions of non-participating molecules fixed. These Grotthuss events were followed by the next MD segment, and so on. Similar concepts, with alternation between short MD segments and proton redistribution in fixed intervals, have been used in previous simulations (albeit for other applications).[38, 41, 81-83]

Anatomy of a Proton Hopping Event. Each $H_3O^+ + H_2O \rightarrow H_2O + H_3O^+$ transition was initiated by identifying the nearest neighbor H_2O for each of the three H_3O^+ hydrogens (Figure 1A). These waters represent the possible acceptors where the proton can end up after a single hop in the Eigen complex.[6, 8, 14, 15] For identifying the most favorable acceptor, one has to consider that the motions

of charged particles (including proton hopping) are subject to electrostatic forces arising from all other partial and ionic charges in the system.[84] For example, if there is another cation in close proximity to a H_3O^+, electrostatic repulsion will favor proton hopping in a direction that increases the distance between the two charges. These electrostatic effects are particularly important for highly charged droplets, where the H_3O^+ behavior is heavily affected by repulsion from other excess ions. To capture the central role of these electrostatics, we surmise that proton hopping will tend to proceed toward the site with the lowest electrostatic potential.

Using electrostatics as key selection criterion implies that our method will not always pick the "special partner", i.e., the H_2O closest to H_3O^+.[80] Our strategy is nonetheless a reasonable approximation because the identity of the special partner alternates between the three H_2O within tens of fs ("special pair dance", Figure S2).[8, 13] Thus, even if the electrostatically selected H_2O does not occupy the special partner position at the exact instant when the hop is executed, the H_2O would have attained this position just before or just after the chosen time point.

Partner selection was implemented by calculating the electrostatic potential[84] ϕ_i for the i = 1, 2, 3 possible acceptor H_2O molecules as well as the original H_3O^+ location (ϕ_0) using $\phi_i = (4\pi\varepsilon_0)^{-1} \Sigma_j (q_j / |\mathbf{r}_i - \mathbf{r}_j|)$. The $\mathbf{r}_i$ positions coincided with the four M sites in the ($H_3O^+ \cdot 3H_2O$) complex, because M constitutes the most central moiety in H_2O and H_3O^+ (Figure S1). The q_j and $\mathbf{r}_j$ refer to partial charges and positions of all other atoms in the droplet, including other H_3O^+. In the case of 5 nm droplets with ~17,000 H_2O, this implies that each ϕ_i calculation involves the summation of ~51,000 terms. For each H_3O^+, four such ϕ_i calculations were required per hopping event (because i = 0…3). For convenience, ϕ_i values were then converted according to $V_i = \phi_i \times e$, representing the potential energy V_i of a hypothetical $+e$ test charge located at $\mathbf{r}_i$ (kJ mol^{-1}). Out of the three candidates, the H_2O with the lowest V_i was selected as proton acceptor for the hopping event (Figure

1B). To ensure that the acceptor selection reflects the wider electrostatic environment of the H_3O^+ (rather than electrostatic forces within the Eigen complex), the 13 atoms of the currently considered ($H_3O^+ \cdot 3H_2O$) moiety were excluded from the ϕ_i calculations. Our acceptor selection method does not consider solvent relaxation, an effect that would lower all three V_i values.[31] We posit that relaxation-induced ΔV_i terms would be similar for all three sites, such that the most suitable acceptor can be selected while keeping the surrounding water immobilized. Inclusion of solvent relaxation during acceptor selection would dramatically increase the computational cost of our method, precluding its application to large systems. Instead, our method allows the solvent to relax after hopping is complete, once the subsequent MD segment resumes. This is different from QM-based descriptions, where hopping and reorientation of the surrounding water occur in unison.[8, 13, 31] The end result is the same as with the strategy used here, i.e., the proton has been transferred and it has attained a relaxed solvent shell.

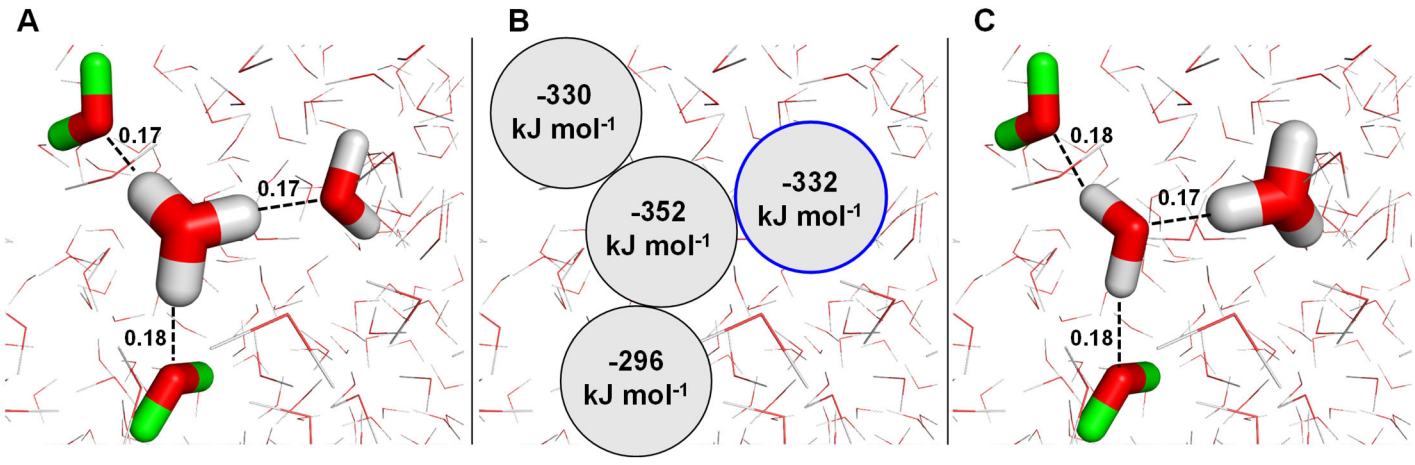

Figure 1. Proton hopping algorithm developed in this work. (A) H_3O^+ with its three nearest-neighbor waters prior to proton hopping. (B) Electrostatic selection of proton acceptor based on V_i energies as described in the text. The most favorable acceptor is highlighted in blue. (C) Newly formed Eigen complex immediately after proton hopping. Non-participating water molecules are shown as lines. Dashed lines represent H-bonds, with numbers that indicate O···H distances in nm.

Hopping was performed by moving the proton from H_3O^+ to the V_i-selected H_2O acceptor (Figure 1C). This was done by leaving both oxygen positions unchanged, and by placing the transferred proton on the O axis. Then, the remaining atoms were repositioned to regenerate proper H_3O^+ and H_2O geometries while ensuring that existing H-bonds with the surrounding water were retained as much as possible (Figures 1C, S4).

Proton Hopping Bursts along Water Wires. The preceding section focused on H_3O^+ hopping to an adjacent water molecule. Interestingly, it has been shown that proton transfer can also occur in "bursts" that involve sub-ps hopping over several H_2O along a water wire. These bursts are followed by "rest" periods of several ps without hopping.[14, 33, 36] We incorporated the possibility of such concerted proton transfer events into our model, using the parameter n_hop_{max} to indicate the maximum number of hops during a burst. AIMD and MS-EVB data suggest $n\_hop_{max} = 5$, and hence we used this value throughout the current work.[14, 33, 36] In agreement with previous investigations,[33, 36] many bursts in our simulations terminated before reaching this maximum value (see *Model Parameters*).

To simulate hopping over multiple water molecules, we subjected each H_3O^+ to the procedure of Figure 1 several times in a row. Figure 2A exemplifies one of these bursts, with proton transfer along five H-bonded H_2O (see Figure S5 for additional details). These events are consistent with the accepted view of the Grotthuss mechanism (Scheme 1).[8, 14, 23-26, 36] If applied without modification, the electrostatic selection of Figure 1 would favor back-and-forth transfer between the same donor/acceptor pair.[33, 36] For our simulations, such "proton rattling"[33, 80] is unproductive because it contributes little to the net translation of H_3O^+, making it difficult to match the experimentally determined diffusion coefficient[18] (for details, see *Model Parameters*). To remedy

this problem we modified the acceptor selection process such that immediate back-and-forth transfer was excluded.

The electrostatic selection strategy of Figure 1 ensures that Grotthuss bursts are subject to other charges in the system. This is illustrated in Figures 2B/C, where the proton trajectory is altered by insertion of a Na^+. In the unmodified system, start and end of this particular trajectory are close together (Figure 2B). The presence of a Na^+ forces the H_3O^+ on a different path that ends with the two ions being far apart. This behavior reflects the repulsion between the two positive charges.

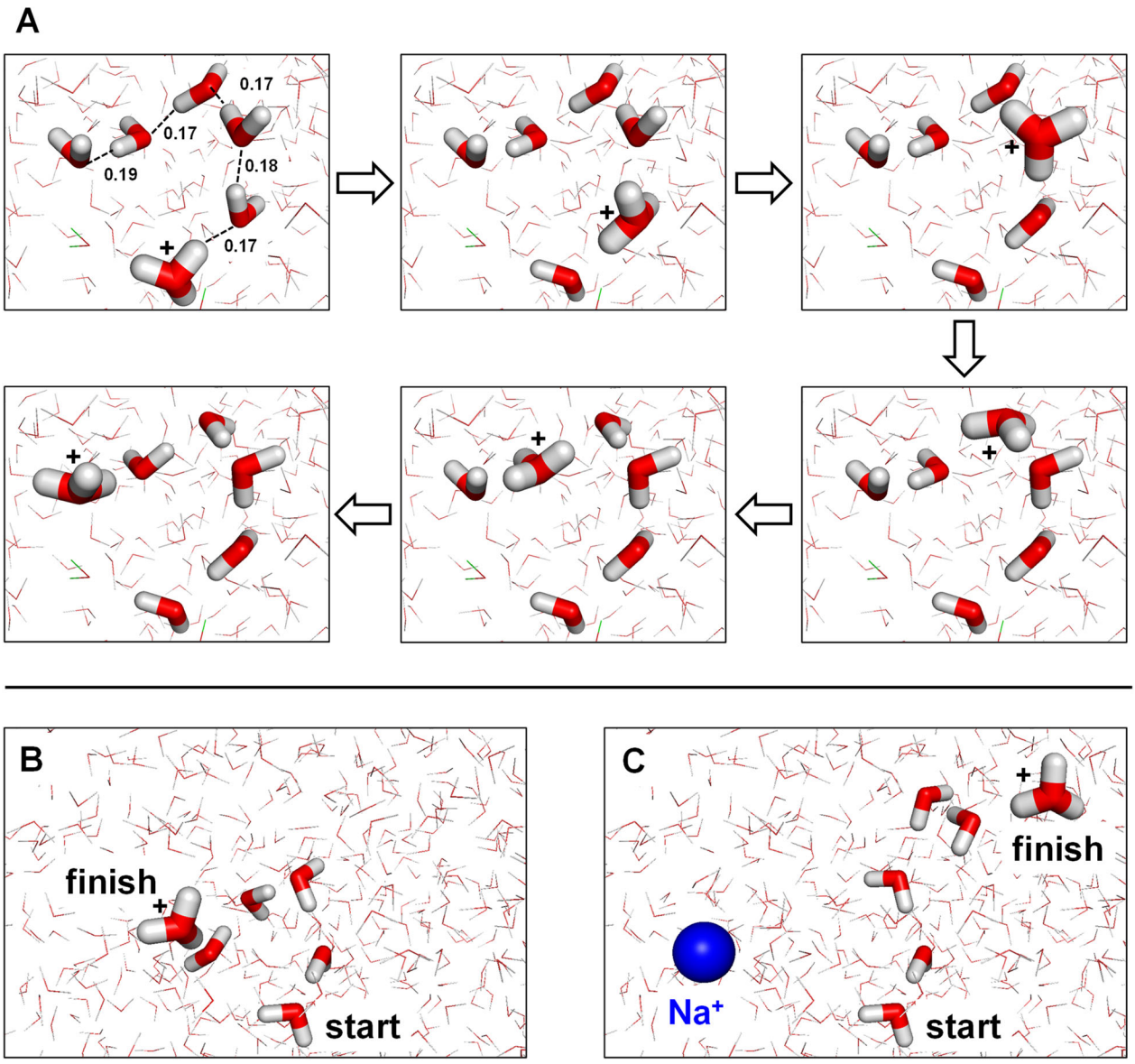

Figure 2. (A) Grotthuss diffusion of H_3O^+ along a water wire consisting of five H_2O. The top left panel illustrates the situation prior to proton hopping, with H-bonds (dashed lines, with bond distances in nm) along the chain of acceptor H_2O molecules. Subsequent panels show proton hopping along this water wire. (B) Water wire after proton hopping from "start" to "finish" during one burst. (C) Same as panel B, except that one Na^+ was added into the system. For all data in this figure the orientation of background water molecules (sticks) remained unchanged. H_3O^+ is highlighted with a "+" symbol in each panel. The data were generated in a droplet with 2 nm radius.

Implementation Details. Simulations were performed using Gromacs 2020.4 with leapfrog integration.[78] Initial droplets were generated by carving a water cube into a sphere with user-defined radius. H_3O^+ or Na^+ were inserted into these initial droplets in random positions. Following steepest descent energy minimization, the temperature was raised to 300 K or 370 K over 200 ps, before commencing production runs. Droplets were simulated for up to 40 ns in a vacuum environment without cutoffs for electrostatic or Lennard-Jones interactions.[63] Temperature control was achieved using the Nosé-Hoover thermostat.[85] As is customary for many MD simulations,[79] high frequency vibrations were eliminated by constraining O-H covalent bonds via the SETTLE[86] and LINCS[87] algorithms for H_2O and H_3O^+, respectively. The constraints permitted a relatively long integration step (2 fs), which is a key requirement for tackling the system size and time windows that are of interest for the current work. The absence of constraints would have required an integration step of 0.5 fs or less, extending the wall clock time at least four-fold.[79] Rayleigh charge calculations for water at 370 K were performed using a surface tension of 0.05891 N m^{-1}.[18] Effective droplet radii were calculated from the droplet mass using a density of 1 g cm^{-3}. Charmm36 Lennard-Jones parameters[88] were used for Na^+ (σ = 0.251367 kJ mol^{-1} and ε = 0.19623 nm).

The simulations were coordinated by a bash script that alternated between Gromacs run segments of duration Δt_hop, and an in-house Python program that performed the Grotthuss events of Figures 1 and 2. A Gromacs-generated coordinate (.gro) file served as input for this Python program, resulting in n_hop_{max} = 5 output .gro files that represent successive stages of proton

hopping bursts. All H_3O^+ were allowed to finish their first hopping event, before proceeding to the second round of hopping etc., until n_hop_{max} = 5 was reached. A hop was not executed if the H O distance was greater than *hop_cutoff*, and no further hopping attempts were made for the corresponding H_3O^+ in that particular burst because the water wire was considered to be broken.[32] To speed up the simulations, the bash script called an in-house Fortran program in 80 ps intervals to eliminate evaporated molecules that had moved more than 15 nm from the droplet center, similar to earlier ESI simulations.[63]

Results and Discussion

The previous sections outline a strategy for Grotthuss MD simulations. Our technique involves short MD segments during which covalent bonds remain intact and all components undergo Brownian motion. These MD segments are interspersed with Grotthuss bursts during which H_3O^+ hop along H-bonded water wires (Figure 1, 2).

Model Parameters. As a first step, we had to choose numerical values for the two adjustable parameters, Δt_hop (the duration of MD segments between proton hopping bursts) and *hop_cutoff* (the maximum allowed H···O distance for each hopping event). Initial clues were taken from the literature. (1) The average interval between proton hops has been suggested to be $\Delta t\_hop \approx$ 1-2 ps, but this value assumes that hopping takes place as isolated donor → acceptor transfer events.[3, 89, 90] When considering that hopping can occur in bursts across up to n_hop_{max} = 5 waters,[14, 33, 36] somewhat longer Δt_hop values should be adequate. Also, longer Δt_hop values are beneficial for our method, because they reduce computational overhead (including Gromacs grompp and mdrun operations[79]), keeping in mind that these operations have to be executed every few ps at the

beginning of each MD segment. (2) Proton transfer is facile if donor and acceptor are in tight H-bonding contact, i.e., ~0.17 nm for "special pair" contacts (Figure S2).[8, 14, 35, 36, 42-44] For longer distances, the chances of a successful hopping event decrease.[26, 91, 92] This implies that *hop_cutoff* will have to be chosen somewhat larger than 0.17 nm.

How can the two aforementioned values be selected? A key benchmark that has to be reproduced in Grotthuss MD simulations is the experimental proton diffusion coefficient $D = 0.0093$ nm^2 ps^{-1} at 300 K.[18] D can be determined by tracking the mean square displacement (*msd*) of a molecule using the relationship $msd(t) = 6Dt$.[38, 42, 93] We conducted simulations where a H_3O^+ was initially placed in the center of a $r = 4$ nm droplet. Multiple runs were performed with various parameter combinations. We settled on $\Delta t\_hop = 4$ ps and *hop_cutoff* = 0.25 nm (with $n\_hop_{max} = 5$ taken from the literature[14, 33, 36]). Grotthuss MD simulations with these parameters yielded $D = 0.0092$ nm^2 ps^{-1}, in close agreement with the experimental value (0.0093 nm^2 ps^{-1}, Figure 3A).[18] Figure 3B shows the probability that $n = 1, \ldots n\_hop_{max}$ hops occur during a Grotthuss burst under these conditions. Consistent with AIMD results,[33] this distribution has its maximum at $n = 1$.

The 0.25 nm *hop_cutoff* is somewhat longer than the ~0.17 nm H O distance of an ideally positioned donor-acceptor "special pair" (Figure S3). The *hop_cutoff* value used here is nonetheless reasonable, considering that our algorithm does not perform solvent relaxation until after a burst is complete (Figures 2, S5). By allowing $n > 1$ proton hopping to proceed even for slightly unfavorable donor-acceptor geometries, our algorithm compensates for this delayed solvent relaxation. As noted earlier, solvent relaxation during proton transfer would dramatically reduce the calculation speed, precluding the application of our method to large systems and long time scales. The relatively high $n = 5$ peak in Figure 3B is somewhat surprising; it reflects the fact that some water wires happen to be in orientations that provide < 0.25 nm hopping distances throughout the entire burst.

We do not claim that the numerical values chosen for Δt_hop and *hop_cutoff* are unique. Equivalent diffusion behavior would presumably be obtained with shorter Δt_hop and a correspondingly smaller *hop_cutoff*. However, such an approach would significantly increase the computational cost of our simulations, as discussed earlier. The parameters used here yield the proper value of D while maintaining computational efficiency.

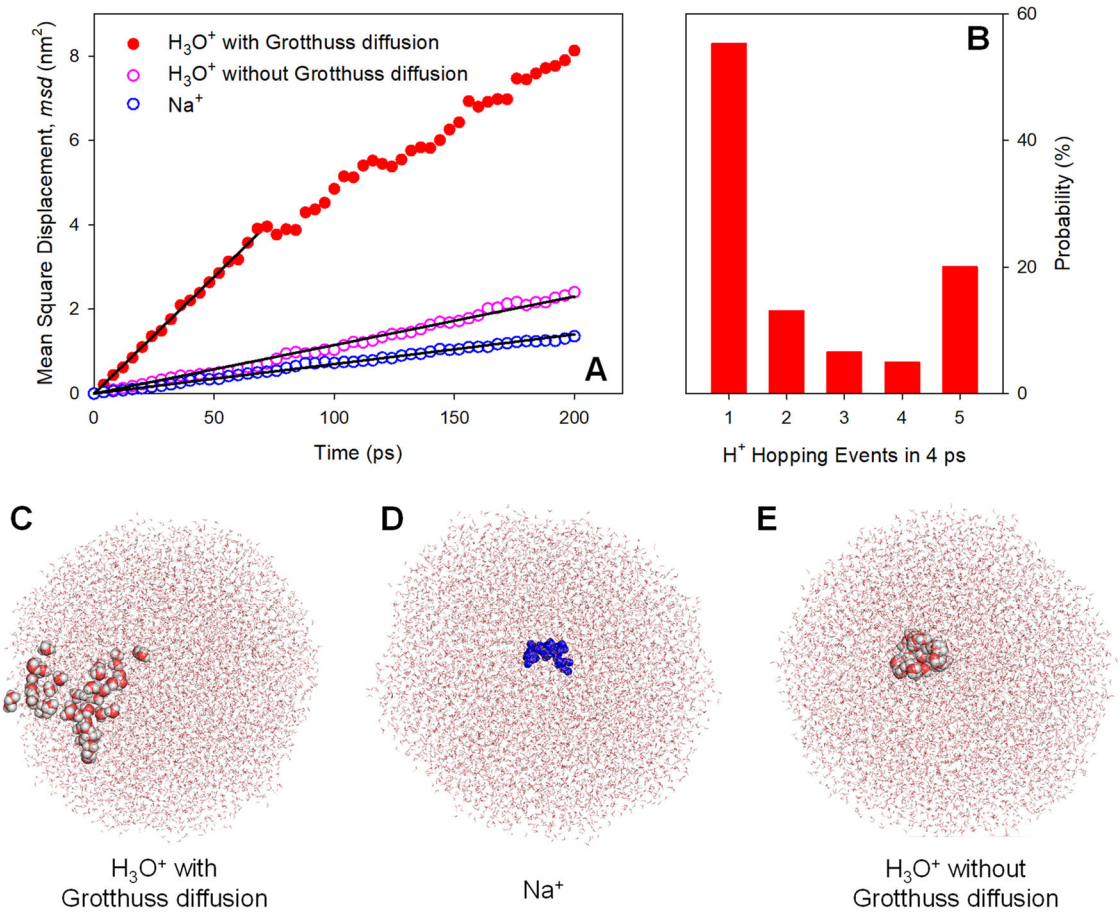

Figure 3. Diffusion simulations of single ions in water droplets (4 nm radius, ~9000 water molecules, 300 K) under different conditions. (A) *msd* vs. time. Dots represent the average of 50 independent runs for each condition, with regression lines from which diffusion coefficients can be determined. Red filled circles: H_3O^+ with Grotthuss diffusion (t > 52 ps data were excluded because of confinement effects at the droplet surface). Blue open circles: Na^+. Pink open circles: H_3O^+ without Grotthuss diffusion. (B) Probability distributions, showing the number of proton hops during Grotthuss bursts. (C) - (E): Representative trajectories under the three conditions of panel A. Each panel shows the initial droplet, as well as the ion positions in 4 ps intervals over 200 ps.

Simulations were also conducted on droplets containing one Na^+, an ion that only undergoes Brownian motion. Those simulations yielded $D = 0.0012$ nm^2 ps^{-1}, close to the Na^+ literature value of 0.0013 nm^2 ps^{-1} (Figure 3A).[18] These Na^+ data do not involve any adjustable parameters, thereby attesting to the appropriateness of the water environment and the diffusion tests used here.

For illustrative purposes we also simulated H_3O^+ without Grotthuss diffusion, which resulted in $D = 0.0019$ nm^2 ps^{-1}. This result is almost five times smaller than the actual proton diffusion coefficient (0.0093 nm^2 ps^{-1}),[18] highlighting how essential it is to include Grotthuss diffusion in H_3O^+ simulations. The dramatically different behavior under the three scenarios explored here is further highlighted in the trajectory snapshots of Figure 3. Grotthuss diffusion allows H_3O^+ to rapidly traverse long distances (Figure 3C), while movement is much more limited for ions that only undergo Brownian motion (Figure 3D, E).

As an additional test, we performed Grotthuss MD simulations under conditions where the H_2O acceptor molecule in $H_3O^+ \cdot 3H_2O$ was randomly selected during each hopping step. With otherwise identical parameters, this random selection yielded $D = 0.0134$ nm^2 ps^{-1} (Figure S6), 46% larger than the proper value (0.0092 nm^2 ps^{-1}) associated with the electrostatic procedure of Figure 1. More importantly, random selection fails to ensure that hopping protons respond to attractive and repulsive forces caused by other charges in the system (Figure 2B, C). All Grotthuss MD data discussed below were therefore generated by applying the electrostatic selection method of Figure 1.

Evaporation of Charged Water Droplets. As noted in the Introduction, electrosprayed water droplets represent an area of particular interest. ESI progeny droplets that release gaseous analyte ions have radii of a few nm and they are highly charged, mainly by excess H_3O^+.[57] Mass

spectrometers employ droplet heating to speed up evaporation. To mimic such conditions, we performed Grotthuss MD simulations at 370 K on droplets with 5 nm radius (~17000 H_2O) and an initial 40+ charge which corresponds to the Rayleigh limit.[57, 59, 60] The focus of the current study is on the H_3O^+ behavior, therefore, our simulated droplets did not include any analytes. Grotthuss MD snapshots for a H_3O^+ containing droplet are shown in Figure 4A. During the 40 ns simulation window the droplets shrank significantly as a result of water evaporation, while maintaining a roughly spherical shape. This was accompanied by occasional H_3O^+ ejection (Figure 4B).

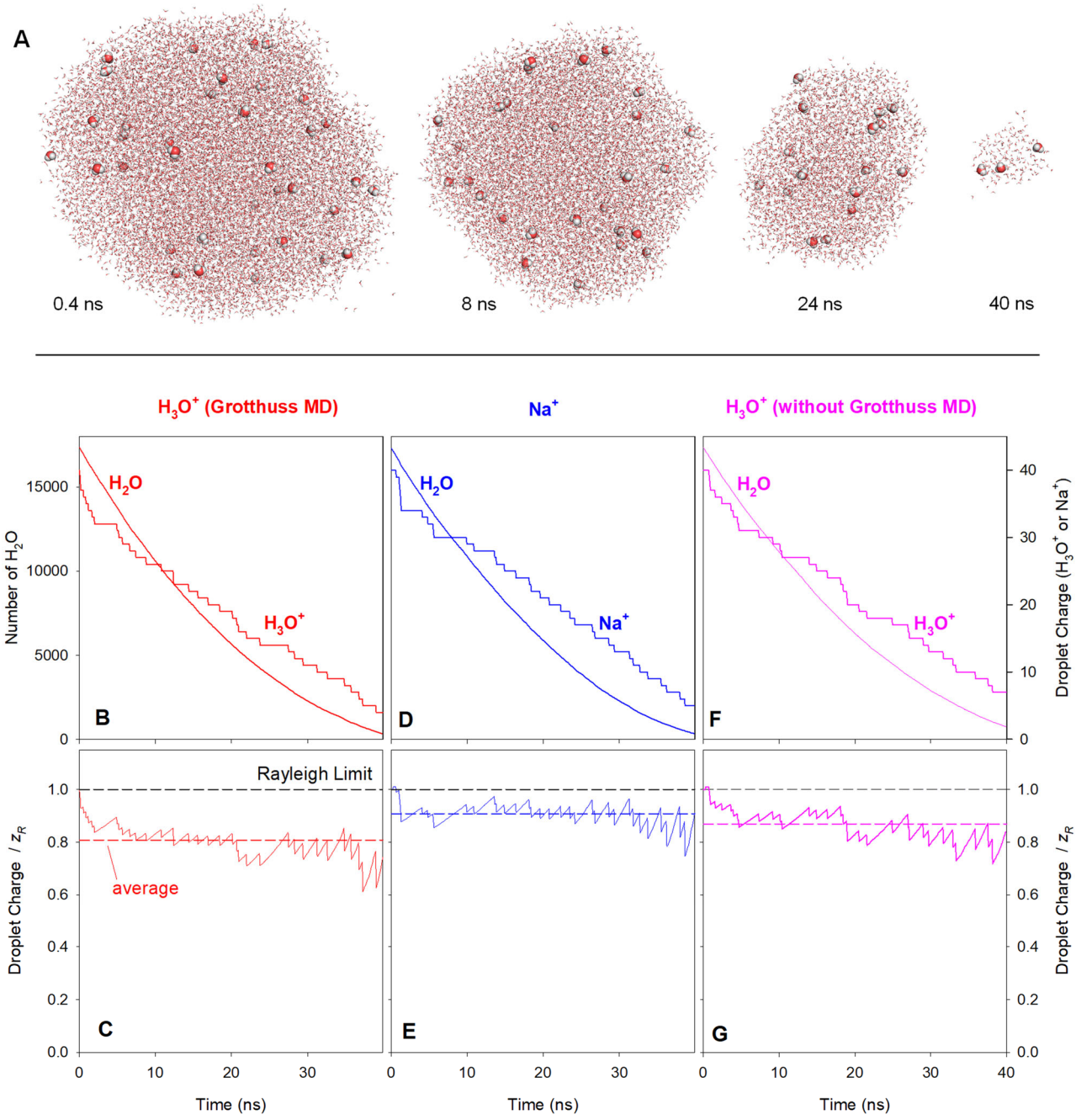

Figure 4. Evaporation and charge loss kinetics for water droplets with an initial radius of 5 nm and an initial 40+ charge at 370 K. (A) Snapshots from a Grotthuss MD simulation on a droplet charged with H_3O^+. (B, C) Composition of the droplet from panel A vs. time. (D, E) Droplet containing Na^+. (F, G) Droplet containing H_3O^+ without Grotthuss MD. Panels along the bottom display the droplet charge z_d relative to the Rayleigh charge z_R. Colored dashed lines display z_d / z_R averages, calculated from three independent MD runs for each condition (see also Figure S7).

Throughout this evaporation/charge ejection process, the droplet charge z_d of the Grotthuss MD runs stayed relatively close to the Rayleigh limit z_R. The average z_d / z_R ratio was 0.81 ± 0.05, with a slight decrease during the 40 ns simulation window (Figure 4C). MD runs on droplets charged with Na^+ showed evaporation kinetics that resembled these Grotthuss MD data (Figure 4D). The relative charge of the Na^+ droplets remained slightly higher (z_d / z_R = 0.91 ± 0.04, Figure 4E) than that of the Grotthuss MD H_3O^+ droplets. For H_3O^+ droplets that were simulated without Grotthuss MD (Figure 4F), the average z_d / z_R was 0.87 ± 0.05 (Figure 4G).

The zigzag appearance of the MD-generated z_d / z_R profiles in Figures 4C,E,G is reminiscent of experimental phase Doppler anemometry data.[59] These profiles reflect the interplay between cohesive interactions within the droplets (mainly H-bonds), and destabilizing charge-charge repulsion among the excess ions.[57, 59] Upward segments of each zigzag profile correspond to solvent evaporation at constant z_d, rendering the droplet more and more labile as it approaches z_R. Sudden downward transitions reflect ion ejection that temporarily stabilizes the droplet by reducing charge-charge repulsion. As seen in Figure 4, these evaporation/ejection events repeat multiple times throughout the droplet life cycle. Experiments have shown that the regime where droplets eject charge depends on the ion type and the solvent properties, ranging from z_d / z_R ≈ 0.6 to 1.2.[60, 94] The z_d / z_R regime seen in our simulations is therefore entirely reasonable (Figures 4C,E,G, see Figure S7 for additional data). In summary, it is gratifying that the z_d / z_R behavior associated with the droplet evaporation (Figure 4C, E, G) is consistent with a wide range of experimental data.[57, 59-61]

Charge Ejection. Ion ejection from charged droplets has been studied extensively. The framework that describes these events is the ion evaporation model (IEM).[63-65, 95-98] Most IEM investigations have focused on metal ions that are ejected with a residual solvent shell. The Na^+ droplets studied

here displayed numerous such IEM events, where a Na^+ approached the droplet surface, formed a small surface protrusion, and subsequently left the droplet bound to a few H_2O (Figure 5D-F).

To the best of our knowledge, IEM events of H_3O^+ under conditions that consider Grotthuss diffusion have not been computationally explored yet. Our Grotthuss MD simulations exhibited an interesting behavior. Similar to Na^+, ejection of H_3O^+ started when an ion approached the droplet periphery and formed a small surface protrusion (Figure 5A). Unlike for Na^+, the occurrence of a Grotthuss burst at this stage can rapidly propel the H_3O^+ to the tip of the protrusion (Figure 5B) from where it leaves the droplet bound to ~6 waters (Figure 5C). Thus, during the IEM ejection of H_3O^+, surface protrusions can act as water wires. Grotthuss migration toward the wire tip is driven by the electrostatic repulsion between the H_3O^+ and the remaining droplet charge. These IEM events are analogous to proton translocation along single-file water chains, as seen previously for smaller systems using AIMD,[99] MS-EVB,[45] and reactive force field simulations.[49]

The rapid Grotthuss transfer of H_3O^+ to the tip of aqueous surface protrusions facilitates ion ejection, providing an explanation for why H_3O^+ droplets undergo IEM events at slightly lower z_d / z_R than Na^+ droplets (Figure 4C, E). An additional contributor to these z_d / z_R differences is the fact that Na^+ is more highly solvated (with a $Na^+ \cdot 6H_2O$ first shell)[100] compared to H_3O^+ where the first solvation shell only comprises three H_2O (Figure 1A).[6, 8, 11, 14] However, this different solvation behavior is a minor factor, as seen by comparing the z_d / z_R regime of the Na^+ droplets with those of non-Grotthuss H_3O^+ data (Figure 4E, G).

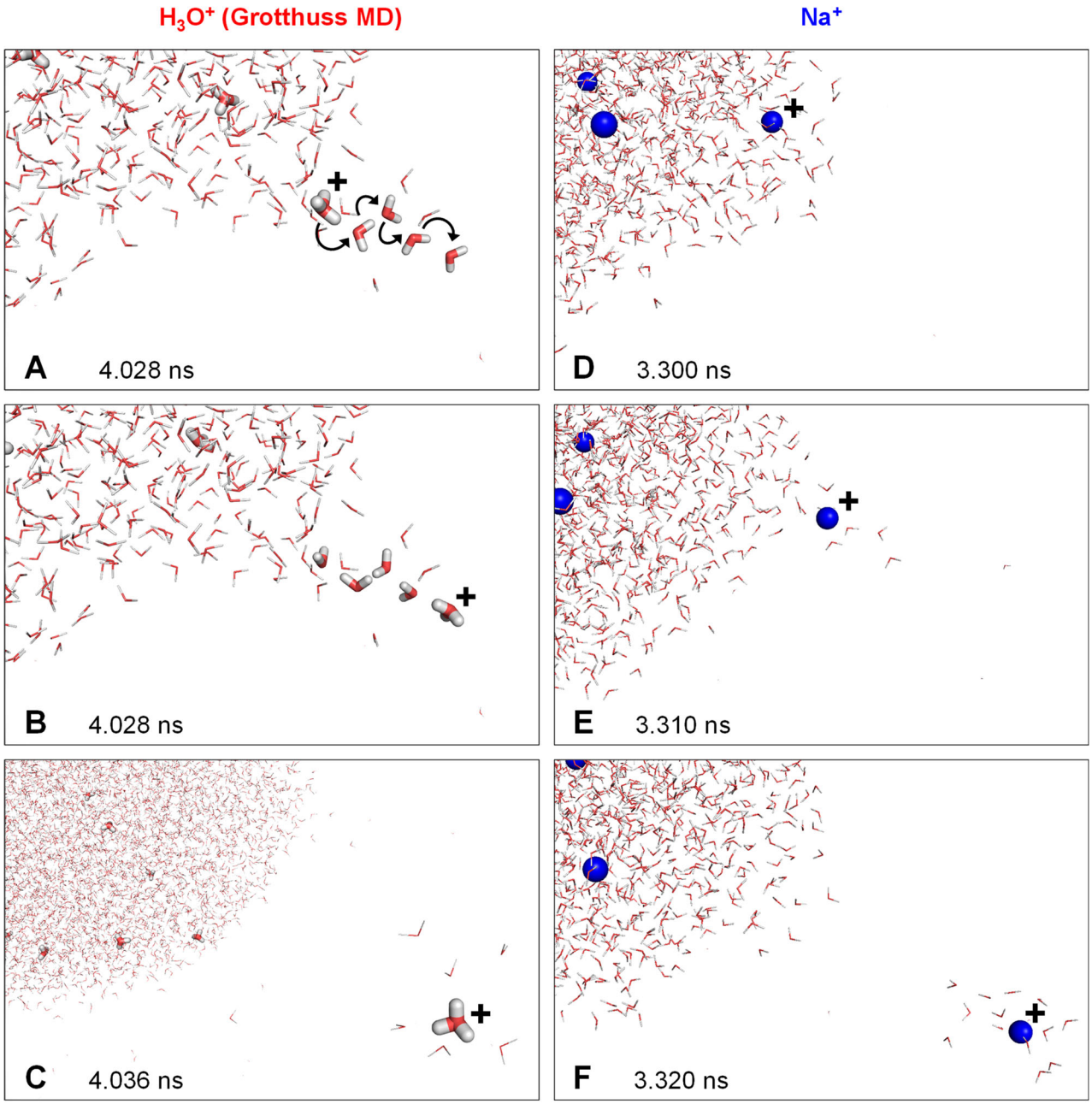

Figure 5. Illustration of charge carrier IEM ejection from aqueous nanodroplets. (A-C) Grotthuss MD of a H_3O^+ containing droplet, resulting in a 31+ → 30+ transition. Curved arrows in panel A indicate covalent bond rearrangements as in Scheme 1; water molecules participating in this Grotthuss chain are highlighted. (D-F) MD simulation of a Na^+ containing droplet, resulting in a 34+ → 33+ transition. The "+" signs in each panel highlight the ion that is being ejected.

H_3O^+ Surface Affinity in Singly Charged Small Clusters. Earlier investigations suggest that small water clusters containing a single H_3O^+ preferentially have this ion located at the surface.[37, 40, 101, 102]

This surface affinity has been attributed to the low electron density of the H_3O^+ oxygen, which renders this atom unable to participate in H-bonding. H_3O^+ therefore only binds three waters (Figure 1A), whereas H_2O can form four H-bonds with its aqueous environment.[31] The overall number of H-bonds in a small cluster is maximized by placing the H_3O^+ at the cluster surface, with the oxygen pointing toward the vapor phase.[37, 103] Experimental verification of this H_3O^+ surface affinity comes from IR spectroscopy on cryogenic clusters, specifically $H_3O^+[H_2O]_{20}$.[11, 12]

To explore the behavior of such small cryogenic systems, we performed Grotthuss MD on $H_3O^+[H_2O]_{20}$ at 300 K with subsequent cooling to 1 K. The resulting cluster structure was very similar to the IR-derived data,[11, 12] with H_3O^+ at the cluster surface and the H_3O^+ oxygen pointing toward the vapor phase (Figure S8). It is reassuring that our simulations reproduce the experimental behavior[11, 12] as well as the AIMD predictions.[37] In contrast to the high surface affinity of H_3O^+, cryogenic clusters containing a single metal cation favor interior charge carrier positions.[104]

Radial Positioning of H_3O^+ in Highly Charged Large Droplets. We now return to the highly charged 370 K droplets of Figures 4 and 5, focusing on spatial ion distributions. Radial distribution functions (RDFs) generated under the three simulation conditions were relatively similar (Figure 6A-C). All RDFs had a broad maximum close to the droplet periphery, with ion population densities that gradually decreased toward the droplet center. None of the three conditions produced a scenario where charge carriers were confined to the droplet surface. Previous droplet simulations involving Na^+ and other non-Grotthuss ions produced RDFs consistent with those of Figure 6B,[64, 73, 105] although the RDFs depend somewhat on the ion type and the MD conditions used.

Close examination of the RDFs in Figure 6 reveals subtle differences. Of the three scenarios, the Grotthuss MD droplets had their H_3O^+ RDF maximum closest to the surface, at $r \approx 4.3$ nm. The Na^+ value was 4.0 nm, and for non-Grotthuss H_3O^+ it was 4.1 nm (dashed lines in Figure 6). With

Grotthuss MD, H_3O^+ thus retained a somewhat elevated surface affinity, although the effect was less pronounced than for small cryogenic clusters (Figure S8).

Why is the H_3O^+ surface affinity lower in the large 370 K droplets? Several factors can be considered. (1) Elevated temperature enhances the Boltzmann population of high energy states, allowing the droplets to sample more of their conformational space. (2) The H_3O^+ surface affinity in small clusters is linked to a specific orientation where the hydronium oxygen points away from the center.[37] Maintaining such a stable orientation in the highly dynamic water environment at 370 K is not feasible. Moreover, the large positive droplet charge disfavors surface dipole orientations where the hydronium oxygen points away from the positive droplet interior. (3) The first solvation shell of ions such as H_3O^+ and Na^+ is surrounded by additional solvation layers, provided that enough solvent molecules are available.[31, 100] Assembly of these extended solvation motifs in the bulk-like interior of the droplet is more facile than at the surface,[104] thereby favoring ion positions that are not directly at the liquid-vapor interface. The combination of these factors causes H_3O^+ to partially penetrate into the droplet interior under the conditions of Figure 6A, instead of being confined to the surface as in the small cryogenic cluster of Figure S8. The lower H_3O^+ surface affinity at 370 K seen in our work is consistent with temperature-dependent MS-EVB simulations (see Fig. 7B in ref.[106]).

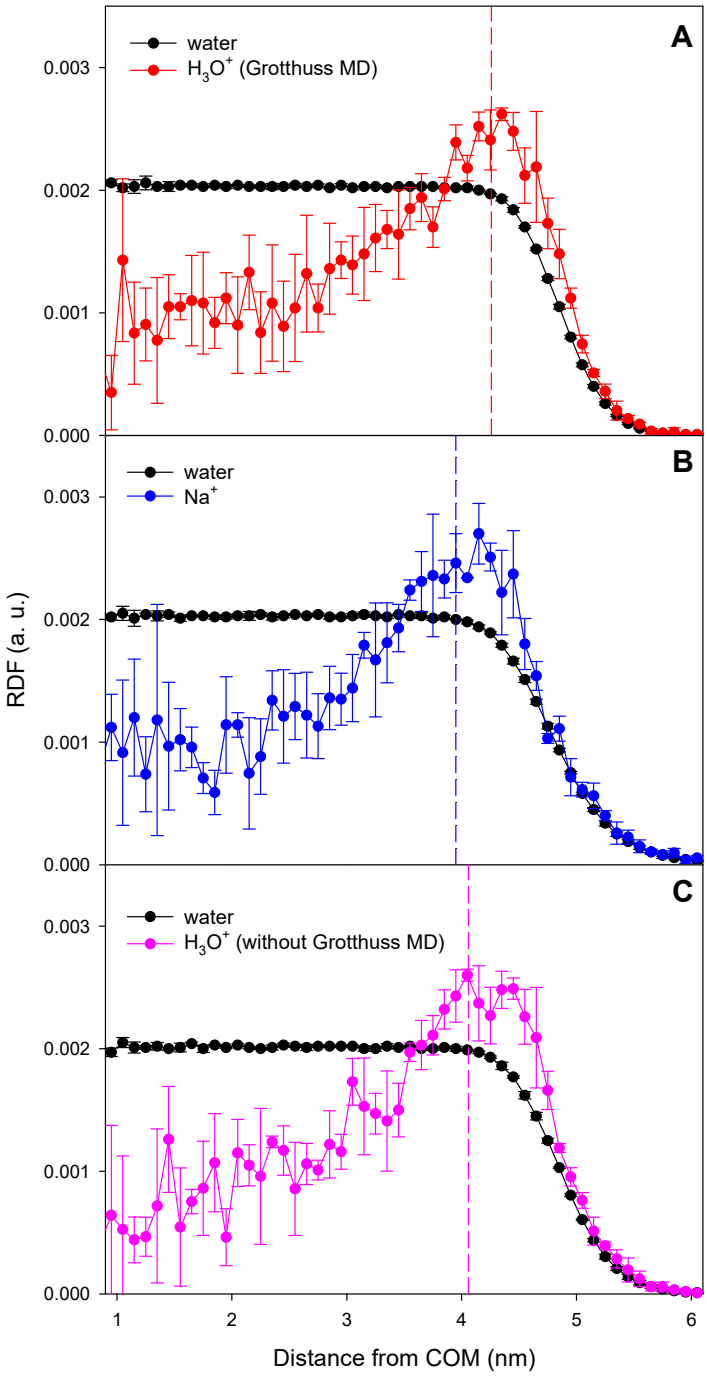

Figure 6. Radial distribution functions (RDFs) describing the composition of charged droplets over the 0 – 4 ns time window at 370 K, following 200 ps of equilibration. Initial droplet radius = 5 nm, initial charge 40+. (A) Droplets containing H_3O^+, using Grotthuss MD. (B) Droplets containing Na^+. (C) Droplets containing H_3O^+ without Grotthuss MD. The data shown here are the average of three independent runs for each condition. Vertical dashed lines indicate approximate peak maxima for charge carrier distributions, calculated as the weighted average of the eleven highest intensity points.

Droplet Surface Charge. Much of the ESI literature has assumed that excess charge carriers reside in a thin layer on the droplet surface.[57, 95, 97, 107] This notion is based on Gauss' Law which states that excess charge on an isolated conductor will move entirely to the conductor surface.[108] At first sight, this surface charge paradigm[57, 95, 97, 107] appears to contradict the data of Figure 6 and previous studies,[64, 73, 105] where excess ions were found to reside throughout the droplet where solvation is more favorable than on the surface. This conundrum was resolved by noting that water and other dipolar solvent molecules align themselves such that the net droplet charge is projected to the surface. Thus, it is the positive ends of orientationally polarized solvent molecules that constitute the surface charge, rather than the excess ions themselves.[73, 105, 109]

It is interesting to examine if this charge projection scenario[73, 105, 109] also holds for H_3O^+ droplets under Grotthuss MD conditions. One way to determine the charge distribution in a droplet is by mapping its electrostatic potential $\phi(r)$, and by comparing the result with theoretical $\phi(r)$ profiles. Any sphere with radius R and net charge Q has an exterior ($r > R$) potential $\phi(r) = kQ/r$, with $k = (4\pi\varepsilon_0)^{-1}$. The interior $\phi(r)$ depends on the spatial charge distribution. Figure 7A illustrates the case where Q is uniformly distributed throughout the volume of the sphere, with $\phi(r) = kQ/2R \times (3 - r^2/R^2)$ for $r \leq R$. In contrast, if Q resides entirely on the surface $\phi(r) = kQ/R = constant$ for $r \leq R$ (Figure 7B).[108]

$\phi(r)$ profiles of MD droplets can be calculated by adding the contributions of all atomic charges.[105] When applying this procedure to Grotthuss MD H_3O^+ droplets (Figure 7C), we found a $\phi(r)$ profile virtually identical to that of Figure 7B. It can be concluded that the Grotthuss MD droplets carry their entire charge on the surface, although many of the H_3O^+ reside in the interior (Figure 6A). As previously discussed for other ions,[73, 105, 109] this phenomenon arises from orientational polarization of the solvent, which projects the interior droplet charge to the surface.

The same behavior was seen for droplets containing Na^+ (Figure 7D), and for H_3O^+ droplets under non-Grotthuss conditions (Figure 7E). Hence, the ability of H_3O^+ to rapidly switch positions by hopping along water wires does not interfere with charge projection to the droplet surface.

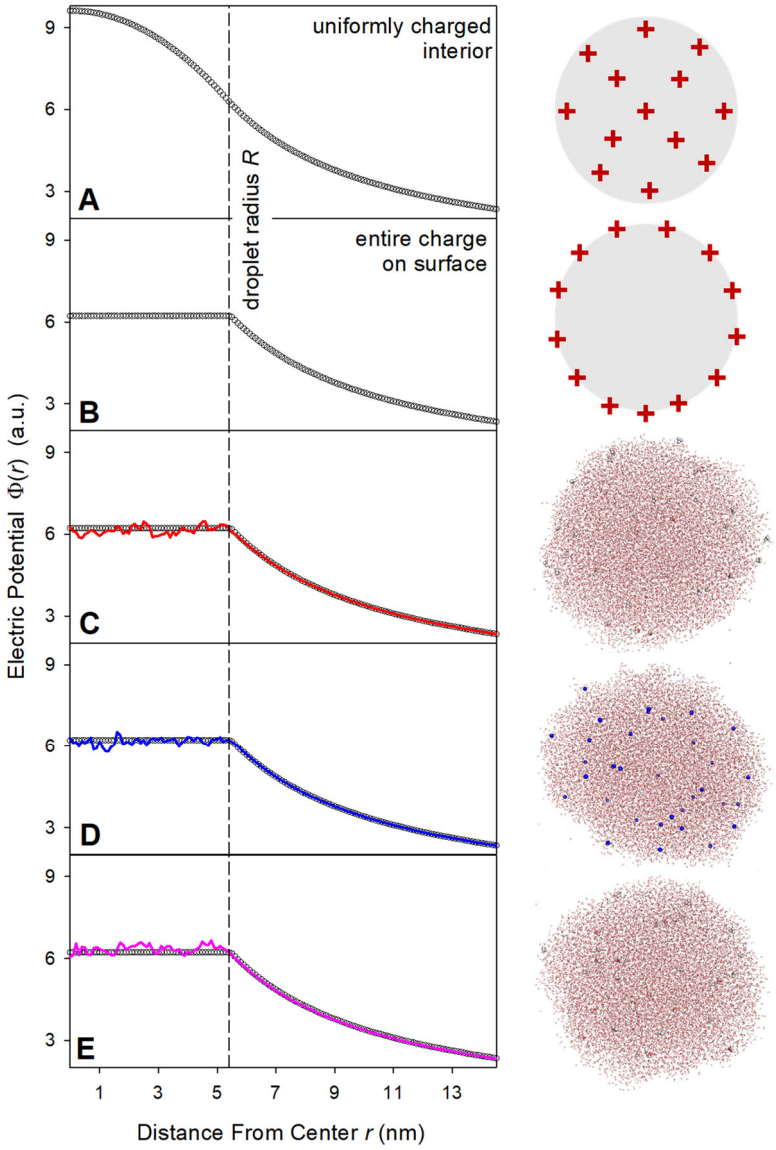

Figure 7. Electrostatic potential $\phi(r)$ in spherical systems that carry a 34+ charge. (A) Sphere with a uniformly charged interior. (B) Sphere that has its entire charge on the surface. (C) Aqueous droplet containing H_3O^+ with Grotthuss MD. (D) Droplet containing Na^+. (E) Droplet containing H_3O^+ without Grotthuss MD. Colored profiles in panels C-E represent MD data; also included in these panels is the "surface charge" $\phi(r)$ from panel B (black). Shown along the right are cartoons or MD structures corresponding to the $\phi(r)$ data. Droplet profiles were generated by averaging five MD frames around 3 ns. $\phi(r)$ calculations used charge in e, distances in nm, and $k = 1$.

Conclusions

The Grotthuss MD technique developed in this work allows simulations on systems that are out of reach for high-level computational methods, significantly expanding the accessible system size and time window. It was not our goal to provide a first-principles description of proton dynamics, an area that requires more intricate techniques such as AIMD,[8, 14, 35-37] QM/MM,[28, 38, 39] and MS-EVB simulations.[8] Instead, we aimed to devise a simple approach that mimics the end result seen with those high-level techniques, i.e., the ability of H_3O^+ to hop along H-bonded water wires. The key features of our method are that it reproduces the experimentally observed proton diffusion coefficient, while accounting for the fact that the hopping direction is governed by electrostatic interactions with other charges in the system. As an added bonus, the method developed here can be readily used in conjunction with the popular Gromacs MD package.[78]

Our model involves two parameters (Δt_hop and *hop_cutoff*) that were adjusted to reproduce the extremely high proton diffusion coefficient observed in experiments.[18] One may ask if the chosen values render other aspects of the model physically unreasonable. Luckily, this is not the case. One critical test concerns the droplet charge. With the chosen parameters, H_3O^+ can rapidly hop to the tip of surface protrusions, with subsequent IEM ejection (Figure 5A-C). It might have been expected that this behavior causes the droplets to lose charge very quickly, resulting in $z_d / z_R \ll 1$. However, such aberrant effects were not observed in our simulations. Instead, the shrinking H_3O^+ droplets remained close to the Rayleigh limit, only slightly below the Na^+ containing systems (Figure 4C, E) and consistent with experiments.[59, 60, 94] Also, the TIP4P/2005 framework reproduced the H_3O^+ equilibrium solvation dynamics quite well (Figures S2, S3), and it captured the surface affinity of H_3O^+ in small cryogenic clusters (Figure S8). All these features serve to validate the strategy used here.

An area that is gradually being conquered by computational chemists are simulations of ESI droplets, and the release of analyte ions into the gas phase.[63-72] Although excess protons play a key role during ESI, none of the previous modeling studies considered Grotthuss diffusion in a realistic fashion. Instead, most earlier ESI simulations focused on droplets charged with metal ions such as Na^+ that can be treated with standard force fields. Luckily, the results of this work indicate that much of the overall droplet behavior is retained when comparing droplets charged with metal ions, and H_3O^+ droplets with Grotthuss diffusion. Both scenarios show solvent evaporation and IEM ejection close to the Rayleigh limit, and both share similar internal ion distributions. It therefore seems that many of the insights and ion formation mechanisms deduced from metal-containing droplets will still hold under conditions that incorporate H_3O^+ with Grotthuss diffusion.

Some additional developments will be required before Grotthuss MD can be applied to ESI scenarios that match typical experimental conditions. Specifically, one has to ensure the participation of analytes and solvent additives such as ammonium acetate[57] in proton hopping, subject to the corresponding pK_a values and hopping rates. It should be relatively straightforward to expand the concepts presented here to such more complex acid/base chemistries. Finally, although the focus of the current work was on droplets, it will be possible to extend Grotthuss MD simulations to bulk systems with periodic boundary conditions. Work in these directions is currently ongoing and will be reported elsewhere.

Supporting Information. Figure S1: Details of H_2O and H_3O^+ models. Figure S2: Special pair dance in $(H_3O^+ \cdot 3H_2O)$. Figure S3: Hydrogen bond distances in $(H_3O^+ \cdot 3H_2O)$. Figure S4: Details of $H_3O^+ + H_2O \rightarrow H_2O + H_3O^+$ proton hopping algorithm. Figure S5: Example of two subsequent proton hopping events. Figure S6: Grotthuss diffusion with electrostatic vs. random acceptor

selection. Figure S7: Relative droplet charge vs. time for various conditions. Figure S8: H_3O^+ $[H_2O]_{20}$ structures.

References

(1) Abrahams, J. P.; Leslie, A. G. W.; Lutter, R.; Walker, J. E. Structure at 2.8 Å resolution of F_1-ATPase from bovine heart mitochondria. *Nature* **1994,** *370*, 621-628.
(2) Arntsen, C.; Savage, J.; Tse, Y. L. S.; Voth, G. A. Simulation of Proton Transport in Proton Exchange Membranes with Reactive Molecular Dynamics. *Fuel Cells* **2016,** *16*, 695-703.
(3) Agmon, N. Elementary steps in excited-state proton transfer. *J. Phys. Chem. A* **2005,** *109*, 13-35.
(4) Stoyanov, E. S.; Stoyanova, I. V.; Reed, C. A. The Structure of the Hydrogen Ion (H-aq(+)) in Water. *J. Am. Chem. Soc.* **2010,** *132*, 1484-+.
(5) Park, M.; Shin, I.; Singh, N. J.; Kim, K. S. Eigen and Zundel forms of smaller protonated water clusters: Structures and infrared spectra. *J. Phys. Chem. A* **2007,** *111*, 10692-10702.
(6) Goyal, P.; Qian, H. J.; Irle, S.; Lu, X. Y.; Roston, D.; Mori, T.; Elstner, M.; Cui, Q. Molecular Simulation of Water and Hydration Effects in Different Environments: Challenges and Developments for DFTB Based Models. *J. Phys. Chem. B* **2014,** *118*, 11007-11027.
(7) Marx, D.; Chandra, A.; Tuckerman, M. E. Aqueous Basic Solutions: Hydroxide Solvation, Structural Diffusion, and Comparison to the Hydrated Proton. *Chem. Rev.* **2010,** *110*, 2174-2216.
(8) Calio, P. B.; Li, C. H.; Voth, G. A. Resolving the Structural Debate for the Hydrated Excess Proton in Water. *J. Am. Chem. Soc.* **2021,** *143*, 18672-18683.
(9) Eigen, M. Proton Transfer, Acid-Base Catalysis, and Enzymatic Hydrolysis. *Angew. Chem.-Int. Edit.* **1964,** *3*, 1-72.
(10) Janoschek, R.; Weideman. E. G.; Pfeiffer, H.; Zundel, G. Extremely High Polarizability of Hydrogen Bonds. *J. Am. Chem. Soc.* **1972,** *94*, 2387-+.
(11) Liu, J.; Yang, J. R.; Zeng, X. C.; Xantheas, S. S.; Yagi, K.; He, X. Towards complete assignment of the infrared spectrum of the protonated water cluster H+(H2O)(21). *Nat. Commun.* **2021,** *12*.
(12) Fournier, J. A.; Johnson, C. J.; Wolke, C. T.; Weddle, G. H.; Wolk, A. B.; Johnson, M. A. Vibrational spectral signature of the proton defect in the three-dimensional H+(H2O)(21) cluster. *Science* **2014,** *344*, 1009-1012.
(13) Markovitch, O.; Chen, H.; Izvekov, S.; Paesani, F.; Voth, G. A.; Agmon, N. Special pair dance and partner selection: Elementary steps in proton transport in liquid water. *J. Phys. Chem. B* **2008,** *112*, 9456-9466.
(14) Hassanali, A.; Giberti, F.; Cuny, J.; Kuhne, T. D.; Parrinello, M. Proton transfer through the water gossamer. *Proc. Natl. Acad. Sci. U. S. A.* **2013,** *110*, 13723-13728.
(15) Swanson, J. M. J.; Simons, J. Role of Charge Transfer in the Structure and Dynamics of the Hydrated Proton. *J. Phys. Chem. B* **2009,** *113*, 5149-5161.
(16) Thamer, M.; De Marco, L.; Ramasesha, K.; Mandal, A.; Tokmakoff, A. Ultrafast 2D IR spectroscopy of the excess proton in liquid water. *Science* **2015,** *350*, 78-82.
(17) Schmitt, U. W.; Voth, G. A. The computer simulation of proton transport in water. *J. Chem. Phys.* **1999,** *111*, 9361-9381.
(18) Lide, D. R., *CRC Handbook of Chemistry and Physics*. 82nd ed.; CRC Press: Boca Raton, London, New York, Washington, 2001.
(19) Adams, E. M.; Hao, H. X.; Leven, I.; Ruttermann, M.; Wirtz, H.; Havenith, M.; Head-Gordon, T. Proton Traffic Jam: Effect of Nanoconfinement and Acid Concentration on Proton Hopping Mechanism. *Angew. Chem.-Int. Edit.* **2021,** *60*, 25419-25427.
(20) Asthana, A.; Wheeler, D. R. A polarizable reactive force field for water to enable molecular dynamics simulations of proton transport. *J. Chem. Phys.* **2013,** *138*, 13.
(21) Grotthuss, C. J. T. Sur la décomposition de l'eau et des corps qu'elle tient en dissolution à l'aide de l'électricité galvanique. *Ann. Chim.* **1806,** *58*, 54-73.
(22) Agmon, N. The Grotthuss Mechanism. *Chem. Phys. Lett.* **1995,** *244*, 456-462.

(23) Cukierman, S. Et tu, Grotthuss! and other unfinished stories. *Biochim. Biophys. Acta* **2006,** *1757*, 876-885.
(24) Marx, D. Proton transfer 200 years after von Grotthuss: Insights from Ab initio simulations. *ChemPhysChem.* **2006,** *7*, 1848-1870.
(25) Brini, E.; Fennell, C. J.; Fernandez-Serra, M.; Hribar-Lee, B.; Luksic, M.; Dill, K. A. How Water's Properties Are Encoded in Its Molecular Structure and Energies. *Chem. Rev.* **2017,** *117*, 12385-12414.
(26) Miyake, T.; Rolandi, M. Grotthuss mechanisms: from proton transport in proton wires to bioprotonic devices. *J. Phys.-Condes. Matter* **2016,** *28*.
(27) Knight, C.; Voth, G. A. The Curious Case of the Hydrated Proton. *Accounts Chem. Res.* **2012,** *45*, 101-109.
(28) Walker, A. R.; Wu, B. N.; Meisner, J.; Fayer, M. D.; Martinez, T. J. Proton Transfer from a Photoacid to a Water Wire: First Principles Simulations and Fast Fluorescence Spectroscopy. *J. Phys. Chem. B* **2021,** *125*, 12539-12551.
(29) Peng, Y. X.; Swanson, J. M. J.; Kang, S. G.; Zhou, R. H.; Voth, G. A. Hydrated Excess Protons Can Create Their Own Water Wires. *J. Phys. Chem. B* **2015,** *119*, 9212-9218.
(30) Cuny, J.; Hassanali, A. A. Ab Initio Molecular Dynamics Study of the Mechanism of Proton Recombination with a Weak Base. *J. Phys. Chem. B* **2014,** *118*, 13903-13912.
(31) Lapid, H.; Agmon, N.; Petersen, M. K.; Voth, G. A. A bond-order analysis of the mechanism for hydrated proton mobility in liquid water. *J. Chem. Phys.* **2005,** *122*, 11.
(32) Nagle, J. F.; Morowitz, H. J. Molecular mechanisms for proton transport in membranes. *Proc. Natl. Acad. Sci. U.S.A.* **1978,** *75*, 298-302.
(33) Arntsen, C.; Chen, C.; Calio, P. B.; Li, C. H.; Voth, G. A. The hopping mechanism of the hydrated excess proton and its contribution to proton diffusion in water. *J. Chem. Phys.* **2021,** *154*, 11.
(34) Tse, Y. L. S.; Knight, C.; Voth, G. A. An analysis of hydrated proton diffusion in ab initio molecular dynamics. *J. Chem. Phys.* **2015,** *142*, 13.
(35) Marx, D.; Tuckerman, M. E.; Hutter, J.; Parrinello, M. The nature of the hydrated excess proton in water. *Nature* **1999,** *397*, 601-604.
(36) Chen, M.; Zheng, L. X.; Santra, B.; Ko, H. Y.; DiStasio, R. A.; Klein, M. L.; Car, R.; Wu, X. F. Hydroxide diffuses slower than hydronium in water because its solvated structure inhibits correlated proton transfer. *Nat. Chem.* **2018,** *10*, 413-419.
(37) Iyengar, S. S.; Day, T. J. F.; Voth, G. A. On the amphiphilic behavior of the hydrated proton: an ab initio molecular dynamics study. *Int. J. Mass Spectrom.* **2005,** *241*, 197-204.
(38) Lill, M. A.; Helms, V. Molecular dynamics simulation of proton transport with quantum mechanically derived proton hopping rates (Q-HOP MD). *J. Chem. Phys.* **2001,** *115*, 7993-8005.
(39) Pezeshki, S.; Lin, H. Adaptive-Partitioning QM/MM for Molecular Dynamics Simulations: 4. Proton Hopping in Bulk Water. *J. Chem. Theo. Comp.* **2015,** *11*, 2398-2411.
(40) Wolf, M. G.; Groenhof, G. Explicit Proton Transfer in Classical Molecular Dynamics Simulations. *J. Comput. Chem.* **2014,** *35*, 657-671.
(41) Lazaridis, T.; Hummer, G. Classical Molecular Dynamics with Mobile Protons. *J. Chem Inf. Model.* **2017,** *57*, 2833-2845.
(42) Boero, M.; Ikeshoji, T.; Terakura, K. Density and temperature dependence of proton diffusion in water: A first-principles molecular dynamics study. *ChemPhysChem* **2005,** *6*, 1775-1779.
(43) Talachutla, S.; Bhat, S.; Duster, A. W.; Lin, H. Improved indicator algorithms for tracking a hydrated proton as a local structural defect in Grotthuss diffusion in aqueous solutions. *Chem. Phys. Lett.* **2021,** *784*, 6.
(44) Park, K.; Lin, W.; Paesani, F. A Refined MS-EVB Model for Proton Transport in Aqueous Environments. *J. Phys. Chem. B* **2012,** *116*, 343-352.
(45) Li, C. H.; Voth, G. A. A quantitative paradigm for water-assisted proton transport through proteins and other confined spaces. *Proc. Natl. Acad. Sci. U. S. A.* **2021,** *118*, 8.
(46) Wu, Y. J.; Chen, H. N.; Wang, F.; Paesani, F.; Voth, G. A. An improved multistate empirical valence bond model for aqueous proton solvation and transport. *J. Phys. Chem. B* **2008,** *112*, 467-482.
(47) Schmidt, R. G.; Brickmann, J. Molecular dynamics simulation study of a hydronium ion in liquid water with implementation of the proton transfer by means of a hopping mechanism. *Solid State Ion.* **1995,** *77*, 3-9.
(48) Xu, Z.-H.; Meuwly, M. Multistate Reactive Molecular Dynamics Simulations of Proton Diffusion in Water Clusters and in the Bulk. *J. Phys. Chem. B* **2019,** *123*, 9846-9861.
(49) Pomes, R.; Roux, B. Molecular mechanism of H+ conduction in the single-file water chain of the gramicidin channel. *Biophys. J.* **2002,** *82*, 2304-2316.
(50) Ahadi, E.; Konermann, L. Molecular Dynamics Simulations of Electrosprayed Water Nanodroplets: Internal Potential Gradients, Location of Excess Charge Centers, and "Hopping" Protons. *J. Phys. Chem. B* **2009,** *113*, 7071-7080.

(51) Hiraoka, K.; Ninomiya, S.; Rankin-Turner, S.; Akashi, S. Comparative study of H3O+ (aq) and NH4+ (aq) on electrophoresis, protonating ability, and sodiation of proteins. *Int. J. Mass Spectrom.* **2022,** *471*, 8.
(52) Raab, S. A.; El-Baba, T. J.; Laganowsky, A.; Russell, D. H.; Valentine, S. J.; Clemmer, D. E. Protons Are Fast and Smart; Proteins Are Slow and Dumb: On the Relationship of Electrospray Ionization Charge States and Conformations. *J. Am. Soc. Mass Spectrom.* **2021,** *32*, 1553-1561.
(53) Hebert, M. J.; Russell, D. H. Tracking the Structural Evolution of 4-Aminobenzoic Acid in the Transition from Solution to the Gas Phase. *J. Phys. Chem. B* **2020,** *124*, 2081-2087.
(54) Ryding, M. J.; Andersson, P. U.; Zatula, A. S.; Uggerud, E. Proton mobility in water clusters. *Eur. J. Mass Spectrom.* **2012,** *18*, 215-222.
(55) Fenn, J. B. Electrospray Wings for Molecular Elephants (Nobel Lecture). *Angew. Chem. Int. Ed.* **2003,** *42*, 3871-3894.
(56) Mann, M. The ever expanding scope of electrospray mass spectrometry-a 30 year journey. *Nat. Commun.* **2019,** *10*.
(57) Kebarle, P.; Verkerk, U. H. Electrospray: From Ions in Solutions to Ions in the Gas Phase, What We Know Now. *Mass Spectrom. Rev.* **2009,** *28*, 898-917.
(58) Cech, N. B.; Enke, C. G. Practical Implication of Some Recent Studies in Electrospray Ionization Fundamentals. *Mass Spectrom. Rev.* **2001,** *20*, 362-387.
(59) Grimm, R. L.; Beauchamp, J. L. Evaporation and Discharge Dynamics of Highly Charged Multicomponent Droplets Generated by Electrospray Ionization. *J. Phys. Chem. A* **2010,** *114*, 1411-1419.
(60) Harper, C. C.; Brauer, D. D.; Francis, M. B.; Williams, E. R. Direct observation of ion emission from charged aqueous nanodrops: effects on gaseous macromolecular charging. *Chem. Sci.* **2021,** *12*, 5185-5195.
(61) de la Mora, J. F. Electrospray Ionization of large multiply charged species proceeds via Dole's charged residue mechanism. *Anal. Chim. Acta* **2000,** *406*, 93-104.
(62) Van Berkel, G. J.; Kertesz, V. Using the Electrochemistry of the Electrospray Ion Source. *Anal. Chem.* **2007,** *79*, 5511-5520.
(63) Aliyari, E.; Konermann, L. Formation of Gaseous Proteins via the Ion Evaporation Model (IEM) in Electrospray Mass Spectrometry. *Anal. Chem.* **2020,** *92*, 10807-10814.
(64) Znamenskiy, V.; Marginean, I.; Vertes, A. Solvated Ion Evaporation from Charged Water Droplets. *J. Phys. Chem. A* **2003,** *107*, 7406-7412.
(65) Caleman, C.; van der Spoel, D. Evaporation from water clusters containing singly charged ions. *Phys. Chem. Chem. Phys.* **2007,** *9*, 5105-5111.
(66) Consta, S.; Oh, M. I.; Kwan, V.; Malevanets, A. Strengths and Weaknesses of Molecular Simulations of Electrosprayed Droplets. *J. Am. Soc. Mass Spectrom.* **2018,** *29*, 2287-2296.
(67) Kim, D.; Wagner, N.; Wooding, K.; Clemmer, D. E.; Russell, D. H. Ions from Solution to the Gas Phase: A Molecular Dynamics Simulation of the Structural Evolution of Substance P during Desolvation of Charged Nanodroplets Generated by Electrospray Ionization. *J. Am. Chem. Soc.* **2017,** *139*, 2981-2988.
(68) Higashi, H.; Tokumi, T.; Hogan, C. J.; Suda, H.; Seto, T.; Otani, Y. Simultaneous ion and neutral evaporation in aqueous nanodrops: experiment, theory, and molecular dynamics simulations. *Phys. Chem. Chem. Phys.* **2015,** *17*, 15746-15755.
(69) Beveridge, R.; Migas, L. G.; Das, R. K.; Pappu, R. V.; Kriwacki, R. W.; Barran, P. E. Ion Mobility Mass Spectrometry Uncovers the Impact of the Patterning of Oppositely Charged Residues on the Conformational Distributions of Intrinsically Disordered Proteins. *J. Am. Chem. Soc.* **2019,** *141*, 4908-4918.
(70) Calixte, E. I.; Liyanage, O. T.; Kim, H. J.; Ziperman, E. D.; Pearson, A. J.; Gallagher, E. S. Release of Carbohydrate-Metal Adducts from Electrospray Droplets: Insight into Glycan Ionization by Electrospray. *J. Phys. Chem. B* **2020,** *124*, 479-486.
(71) Kondalaji, S. G.; Khakinejad, M.; Valentine, S. J. Comprehensive Peptide Ion Structure Studies Using Ion Mobility Techniques: Part 3. Relating Solution-Phase to Gas-Phase Structures. *J. Am. Soc. Mass Spectrom.* **2018,** *29*, 1665-1677.
(72) Porrini, M.; Rosu, F.; Rabin, C.; Darre, L.; Gomez, H.; Orozco, M.; Gabelica, V. Compaction of Duplex Nucleic Acids upon Native Electrospray Mass Spectrometry. *ACS Central Sci.* **2017,** *3*, 454–461.
(73) Kwan, V.; Consta, S. Molecular Characterization of the Surface Excess Charge Layer in Droplets. *J. Am. Soc. Mass Spectrom.* **2021,** *32*, 33-45.
(74) Abascal, J. L. F.; Vega, C. A general purpose model for the condensed phases of water: TIP4P/2005. *J. Chem. Phys.* **2005,** *123*, 234505.
(75) Vega, C.; de Miguel, E. Surface tension of the most popular models of water by using the test-area simulation method. *J. Chem. Phys.* **2007,** *126*, 154707.

(76) Temelso, B.; Koddermann, T.; Kirschner, K. N.; Klein, K.; Shields, G. C. Structure and thermodynamics of H3O+(H2O)(8) clusters: A combined molecular dynamics and quantum mechanics approach. *Comput. Theor. Chem.* **2013,** *1021*, 240-248.
(77) Kusaka, I.; Wang, Z. G.; Seinfeld, J. H. Binary nucleation of sulfuric acid-water: Monte Carlo simulation. *J. Chem. Phys.* **1998,** *108*, 6829-6848.
(78) Abraham, M. J.; Murtola, T.; Schulz, R.; Páll, S.; Smith, J. C.; Hess, B.; Lindahl, E. GROMACS: High performance molecular simulations through multi-level parallelism from laptops to supercomputers. *SoftwareX* **2015,** *1–2*, 19-25.
(79) Lindahl, E., In *Molecular Modeling of Proteins. Methods in Molecular Biology (Methods and Protocols)*, Kukol, A., Ed. Humana Press: New York, NY, 2015; Vol. 1215, pp 3-26.
(80) Tuckerman, M. E.; Laasonen, K.; Sprik, M.; Parrinello, M. *Ab initio* molelular dynamics simulation of the solvation and transport of hydronium and hydoroxyl ions in water. *J. Chem. Phys.* **1995,** *103*, 150-161.
(81) Fegan, S. K.; Thachuk, M. A Charge Moving Algorithm for Molecular Dynamics Simulations of Gas-Phase Proteins. *J. Chem. Theory Comput.* **2013,** *9*, 2531-2539.
(82) Konermann, L. Molecular Dynamics Simulations on Gas-Phase Proteins with Mobile Protons: Inclusion of All-Atom Charge Solvation. *J. Phys. Chem. B* **2017,** *121*, 8102-8112.
(83) Goh, G. B.; Hulbert, B. S.; Zhou, H. Q.; Brooks, C. L. Constant pH molecular dynamics of proteins in explicit solvent with proton tautomerism. *Proteins* **2014,** *82*, 1319-1331.
(84) Cisneros, G. A.; Karttunen, M.; Ren, P. Y.; Sagui, C. Classical Electrostatics for Biomolecular Simulations. *Chem. Rev.* **2014,** *114*, 779-814.
(85) Hoover, W. G. Canonical dynamics: Equilibrium phase-space distributions. *Phys. Rev. A* **1985,** *31*, 1695-1697.
(86) Miyamoto, S.; Kollman, P. A. SETTLE: An Analytical Version of the SHAKE and RATTLE Algorithm for Rigid Water Models. *J. Comput. Chem.* **1992,** *13*, 952-962.
(87) Hess, B. P-LINCS: A parallel linear constraint solver for molecular simulation. *J. Chem. Theory Comput.* **2008,** *4*, 116-122.
(88) Huang, J.; MacKerell, A. D. CHARMM36 all-atom additive protein force field: Validation based on comparison to NMR data. *J. Comput. Chem.* **2013,** *34*, 2135-2145.
(89) Luz, Z.; Meiboom, S. The Activation Energies of Proton Transfer Reactions in Water. *J. Am. Chem. Soc.* **1964,** *86*, 4768-4769.
(90) Jungwirth, P.; Tobias, D. J. Specfic ion effects at the air/water interface. *Chem. Rev.* **2006,** *106*, 1259-1281.
(91) Consta, S.; Kapral, R. Proton transfer in mesoscopic, molecular clusters. *J. Chem. Phys.* **1994,** *101*, 10908-10914.
(92) Huneycutt, A. J.; Saykally, R. J. Building solutions - One molecule at a time. *Science* **2003,** *299*, 1329-1330.
(93) Rossky, P. J.; Karplus, M. Solvation. A Molecular Dynamics Study of a Dipeptide in Water. *J. Am. Chem. Soc.* **1979,** *101*, 1913-1937.
(94) Smith, J. N.; Flagan, R. C.; Beauchamp, J. L. Droplet evaporation and discharge dynamics in electrospray ionization. *J. Phys. Chem. A* **2002,** *106*, 9957-9967.
(95) Iribarne, J. V.; Thomson, B. A. On the evaporation of small ions from charged droplets. *J. Chem. Phys.* **1976,** *64*, 2287-2294.
(96) Loscertales, I. G.; de la Mora, J. F. Experiments on the kinetics of field evaporation of small ions from droplets. *J. Chem. Phys.* **1995,** *103*, 5041-5060.
(97) Fenn, J. B.; Rosell, J.; Meng, C. K. In Electrospray Ionization, How Much Pull Does an Ion Need to Escape Its Droplet Prison? *J. Am. Soc. Mass Spectrom.* **1997,** *8*, 1147-1157.
(98) Consta, S. Fragmentation reactions of charged aqueous clusters. *J. Mol. Struct. (Theochem)* **2002,** *591*, 131-140.
(99) Mei, H. S.; Tuckerman, M. E.; Sagnella, D. E.; Klein, M. L. Quantum nuclear ab initio molecular dynamics study of water wires. *J. Phys. Chem. B* **1998,** *102*, 10446-10458.
(100) Marcus, Y. Effect of Ions on the Structure of Water: Structure Making and Breaking. *Chem. Rev.* **2009,** *109*, 1346-1370.
(101) Iyengar, S. S.; Petersen, M. K.; Day, T. J. F.; Burnham, C. J.; Teige, V. E.; Voth, G. A. The properties of ion-water clusters. I. The protonated 21-water cluster. *J. Chem. Phys.* **2005,** *123*, 9.
(102) Hub, J. S.; Wolf, M. G.; Caleman, C.; Maaren, P. J.; Groenhof, G.; van der Spoel, D. Thermodynamics of hydronium and hydroxide surface solvation. *Chem. Sci.* **2014,** *5*, 1745-1749.
(103) Petersen, M. K.; Iyengar, S. S.; Day, T. J. F.; Voth, G. A. The hydrated proton at the water liquid/vapor interface. *J. Phys. Chem. B* **2004,** *108*, 14804-14806.
(104) Cooper, R. J.; O'Brien, J. T.; Chang, T. M.; Williams, E. R. Structural and electrostatic effects at the surfaces of size- and charge-selected aqueous nanodrops. *Chem. Sci.* **2017,** *8*, 5201-5213.

(105) Ahadi, E.; Konermann, L. Surface charge of electrosprayed water nanodroplets: A molecular dynamics study. *J. Am. Chem. Soc.* **2010,** *132*, 11270-11277.
(106) Burnham, C. J.; Petersen, M. K.; Day, T. J. F.; Iyengar, S. S.; Voth, G. A. The properties of ion-water clusters. II. Solvation structures of Na+, Cl-, and H+ clusters as a function of temperature. *J. Chem. Phys.* **2006,** *124*, 024327.
(107) Iavarone, A. T.; Williams, E. R. Mechanism of Charging and Supercharging Molecules in Electrospray Ionization. *J. Am. Chem. Soc.* **2003,** *125*, 2319-2327.
(108) Halliday, D.; Resnick, R.; Krane, K. S., *Physics*. 4 ed.; Wiley: New York, 1992.
(109) Metwally, H.; McAllister, R. G.; Popa, V.; Konermann, L. Mechanism of Protein Supercharging by Sulfolane and m-Nitrobenzyl Alcohol: Molecular Dynamics Simulations of the Electrospray Process. *Anal. Chem.* **2016,** *88*, 5345-5354.

TOC Graphic